



## Enhanced performance of hybrid solar cells based on ordered electrospun ZnO nanofibers modified with CdS on the surface

Sujuan Wu<sup>a,b</sup>, Jinhua Li<sup>a</sup>, Shing-Chung Lo<sup>a</sup>, Qidong Tai<sup>a</sup>, Feng Yan<sup>a,\*</sup>

<sup>a</sup> Department of Applied Physics and Materials Research Center, The Hong Kong Polytechnic University, Kowloon, Hong Kong, China

<sup>b</sup> Laboratory for Advanced Materials, The School of Physics and Telecommunication Engineering, South China Normal University, Guangzhou 510006, China

### ARTICLE INFO

#### Article history:

Received 28 December 2011

Received in revised form 20 April 2012

Accepted 24 April 2012

Available online 11 May 2012

#### Keywords:

Organic solar cell

Electrospun nanofibers

ZnO

CdS

Poly(3-hexylthiophene)

### ABSTRACT

To improve the performance of the hybrid solar cells based on electrospun zinc oxide nanofibers/poly(3-hexylthiophene) (ZnO/P3HT), we modified the ZnO nanofibers with nanocrystalline cadmium sulfide (CdS) by solution process and successfully obtained CdS/ZnO core-shell nanofibers. The CdS modification at the optimum condition can dramatically improve all photovoltaic parameters and increase the power conversion efficiency of the hybrid solar cells for over 100%. In addition, the lifetimes of carriers in the hybrid solar cells characterized by impedance analyzer become much longer after the modification of CdS. The effect of CdS modification on the devices can be mainly attributed to the cascaded energy band structure of the heterojunction that favors charge transport process and thus increases the efficiencies of the devices.

© 2012 Elsevier B.V. All rights reserved.

### 1. Introduction

Organic photovoltaic devices have drawn more and more attention in recent years due to many advantages of the organic devices, such as easy fabrication, flexibility and low cost. Hybrid solar cells based on the composites of n-type inorganic nanomaterials and p-type conjugated polymers are of particular interest because of the relatively high electron mobility, good physical and chemical stability of inorganic materials, and their potential for the production of flexible and large-area solar cells at dramatically low cost [1–12]. However, in such hybrid bulk heterojunction photovoltaic devices, power conversion efficiencies (PCE) are often limited by the poorly formed organic–inorganic interface for electron transfer and the non-continuous electron transport paths in active layers [1–7,13]. Therefore, rigid nanocrystalline structures that present continuous paths for photogenerated electrons to cathode have been popularly used, including template porous structures [14], tetrapods [15], vertically aligned

nanorods [16–21] and electrospun nanofibers [8,9]. It is notable that electrospinning process is a convenient technique for the fabrication of large-area, alignment controllable and low-cost nanofibers that can be used in hybrid solar cells.

ZnO is a good candidate for a n-type semiconductor in hybrid photovoltaic devices because of its high electron mobility, good air stability and appropriate band alignment with conjugated polymers, such as poly(3-hexylthiophene) (P3HT). Various hybrid photovoltaic devices have been developed by incorporating ZnO nanoparticles and nanorod arrays [3,12,16–21]. In our previous report, ordered ZnO nanofibers were fabricated by electrospinning method and used in ZnO/P3HT hybrid solar cells [8]. However, the PCE of all of the above devices based on ZnO nano-materials are still relatively low compared with whole organic solar cells [22–24]. One reason is because ZnO can only absorb and utilize light radiation in the UV region of the solar spectrum due to the wide bandgap. A method to solve this problem is to anchor narrow bandgap sensitizers such as organic dye [9,13] or inorganic semiconductor materials [2,12,25–31] on the surface of ZnO to enhance light harvesting in the visible region, which

\* Corresponding author. Tel.: +852 27664054; fax: +852 23337629.

E-mail address: [apafyan@polyu.edu.hk](mailto:apafyan@polyu.edu.hk) (F. Yan).

encompasses much of the wavelength range of the incident solar spectrum. Compared to organic dyes, inorganic semiconductors have several advantages, such as higher light absorbance, tailoring of optical absorption over a wider wavelength range, and acting as recombination barriers [26,28,29]. Various inorganic materials, such as CdS [27–29], CdSe [12],  $\text{Sb}_2\text{S}_3$  [26,30], and mercurochrome [2], have been used for surface modification in hybrid solar cells.

In the present study, we fabricated ordered ZnO nanofibers by electrospinning method and modified the nanofibers using CdS by nanocrystal layer deposition method [31]. Then we investigated the performance of the hybrid solar cells based on the CdS/ZnO nanofibers and P3HT. The devices have been optimized by changing the number of layers of cross-aligned ZnO nanofibers and the growth time of CdS on ZnO. We found that the PCE of such hybrid solar cell was improved for more than 100% after the modification of CdS. The lifetime of carriers at the bulk heterojunction was characterized by an impedance analyzer and was found to be dramatically increased after the modification of CdS.

## 2. Experimental

### 2.1. Materials

Ordered ZnO nanofibers were deposited on a ZnO-coated ITO glass substrates ( $15 \Omega/\text{sq.}$ ) by electrospinning method as described in our previous paper [8,32]. The electrospinning time for each layer of ZnO nanofibers was controlled to be 30 min. The next layer was deposited with an alignment direction perpendicular to that of the previous one, as shown in Fig. 1.

Then the ZnO nanofibers were modified with CdS by nanocrystal layer deposition method. The nanofibrous films were dipped in an aqueous solution of 10 mM  $\text{Cd}(\text{NO}_3)_2$  and 10 mM thioacetamide at room temperature for different period, which is referred as the growth time for CdS. The CdS shell thickness can be controlled by changing the growth time. The deposition of CdS was indicated by the emergence of yellow color on the surface of ZnO nanofibrous films. Samples were then rinsed thoroughly with deionized water and dried in air.

CdS nanoparticles for TEM characterization were prepared by coating and drying the aqueous solution of 10 mM  $\text{Cd}(\text{NO}_3)_2$  and 10 mM thioacetamide on a glass substrate. Then the CdS nanoparticles were collected from the glass substrate by using a blade and placed on a TEM copper grid covered with carbon film for TEM characterization.

### 2.2. Device fabrication

Fig. 1(a) shows the schematic diagram of the structure of the hybrid solar cells. P3HT was infiltrated into the ZnO nanofibrous films on ZnO-coated ITO glass substrates by spin coating a solution of regioregular P3HT (Reike, regioregularity is  $\sim 93\%$ ) dissolved in toluene (30 mg/ml) followed by a thermal anneal at  $120^\circ\text{C}$  for 20 min in a glovebox filled with high purity nitrogen. The thickness

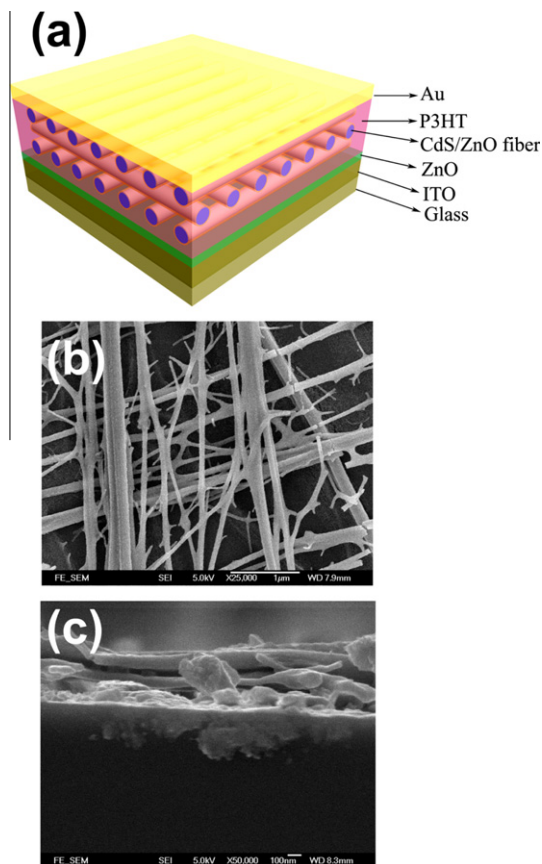


**Fig. 1.** (a) Schematic diagram of a hybrid solar cell based on CdS/ZnO core-shell nanofibers and P3HT. (b) Top view and (c) cross-section view of cross-aligned ZnO nanofibrous films (three layers) modified with CdS (growth time: 5 min) on ITO/glass substrates observed under SEM.

of the P3HT layer was optimized by controlling the spin coating speed. Then a  $\sim 100$  nm Au top electrode was deposited by thermal evaporation through a shadow mask under a vacuum of  $10^{-6}$  mbar. All of the solar cells have the size of  $2 \text{ mm} \times 2 \text{ mm}$ .

### 2.3. Characterization

The photovoltaic performance of the hybrid solar cells was measured by using a Keithley 2400 source meter under an illumination of  $100 \text{ mW}/\text{cm}^2$  (Newport 91160, 300 W solar simulator equipped with an AM1.5 filter). The external quantum efficiency (EQE) of the devices were measured with a standard EQE system, including a xenon lamp (Oriel 66902, 300 W), a monochromator (Newport 66902), a Si detector (Oriel 76175\_71580) and a dual channel power meter (Newport 2931\_C).

Scanning electron microscopy (SEM, Quanta 200 FEG System, FEI Co., USA) and transmission electron microscopy (TEM; F2010, Japan) were used to study the morphology, dimensions, crystallinity, and grain size of ZnO nanofibers and CdS crystallites. The UV-vis absorption spectra of the hybrid films were measured by a SHIMADZU UV-2550 spectrophotometer. The impedances of the devices under different bias voltages were characterized in dark by an

impedance analyzer (HP 4294) in a frequency range from 40 Hz to 20 MHz with an oscillating voltage of 50 mV.

The contact angles of toluene on ZnO and CdS/ZnO films were measured using a standard goniometer (rame-hart inc.) equipped with a microscope and illumination system [33]. The samples were placed on a flat, horizontal support in air.

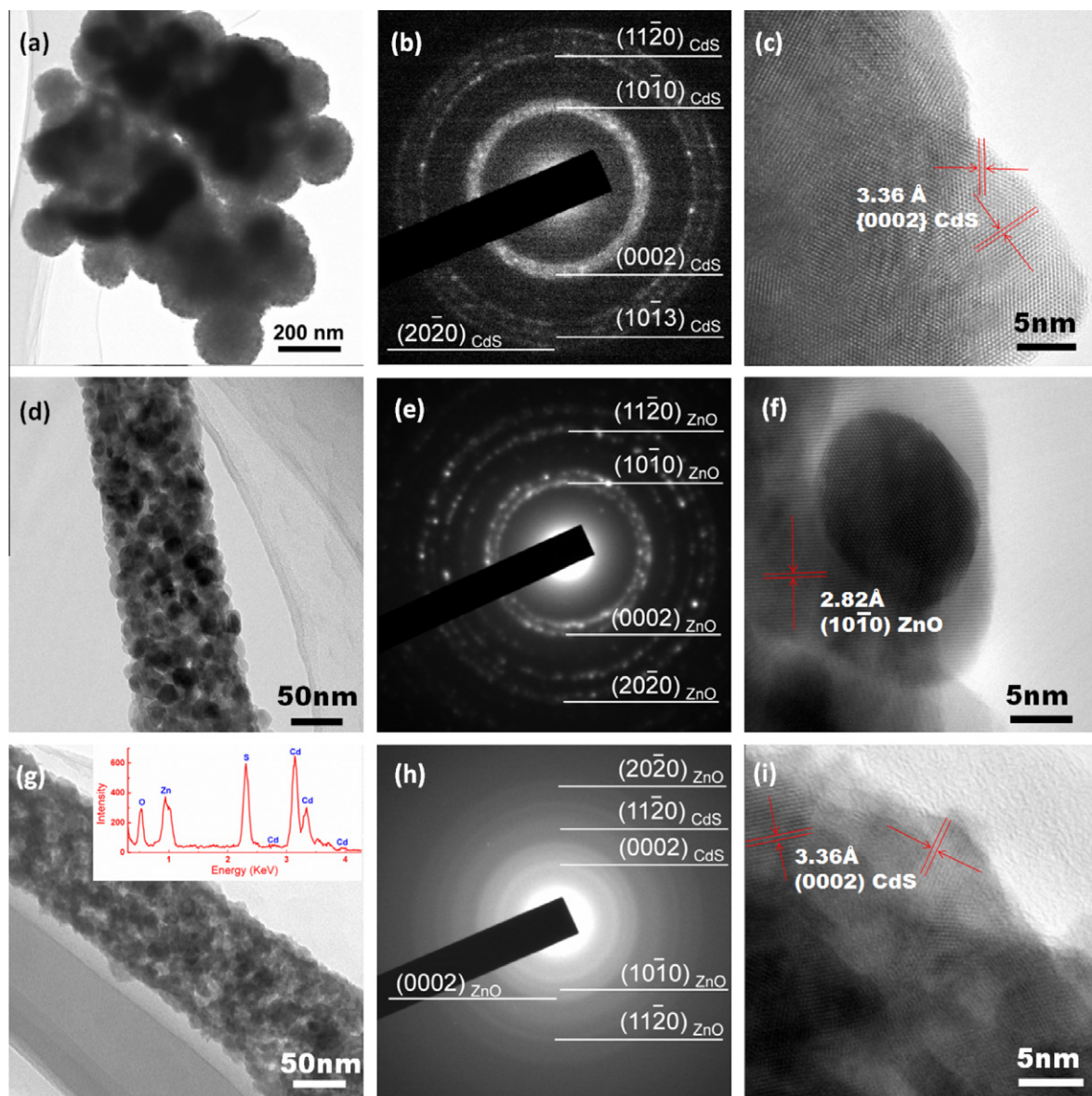
### 3. Results and discussion

Fig. 2(a) and (b) shows a TEM figure and a diffraction pattern of CdS nanoparticles, respectively. The crystal

structure of the CdS nanoparticles is hexagonal wurtzite. Fig. 1(c) shows the high resolution image of CdS nanoparticles.

Fig. 2(d) shows a TEM picture of an electrospun polycrystalline ZnO nanofiber. The diffraction pattern of the ZnO nanofiber is shown in Fig. 2(e). The polycrystalline rings corresponding to different crystal faces of ZnO indicate that the structure of the nanofiber is hexagonal wurtzite. Fig. 2(f) clearly shows the high resolution image of ZnO crystallites.

Fig. 2(g) shows a TEM picture of a CdS-modified ZnO nanofiber. The diffraction pattern of the CdS/ZnO nanofiber shown in Fig. 2(h) exhibits the hexagonal crystal structure



**Fig. 2.** (a) TEM image, (b) selected area electron diffraction (SAED) pattern, and (c) high resolution image of CdS nanoparticles. (d) TEM image, (e) SAED pattern, and (f) high resolution image of an electrospun ZnO nanofiber. (g) TEM image, (h) SAED pattern, and (i) high resolution image of an electrospun ZnO nanofiber modified with CdS (growth time: 5 min) on the surface. The inset of (g) shows the energy dispersive X-ray spectrum of the CdS/ZnO nanofiber, indicating that the fiber contains Zn, O, Cd and S.

of CdS layer while ZnO diffraction pattern becomes very weak [31], which indicates that the ZnO nanofiber was covered with CdS layer. The high resolution image of CdS crystallites is shown in Fig. 2(i). We can clearly see the crystallites of CdS with an average size of about 10 nm grown uniformly and densely on the surface of the ZnO nanofiber. The lattice constant  $c$  of CdS is 6.72 Å, which is very similar to that reported in literatures [31].

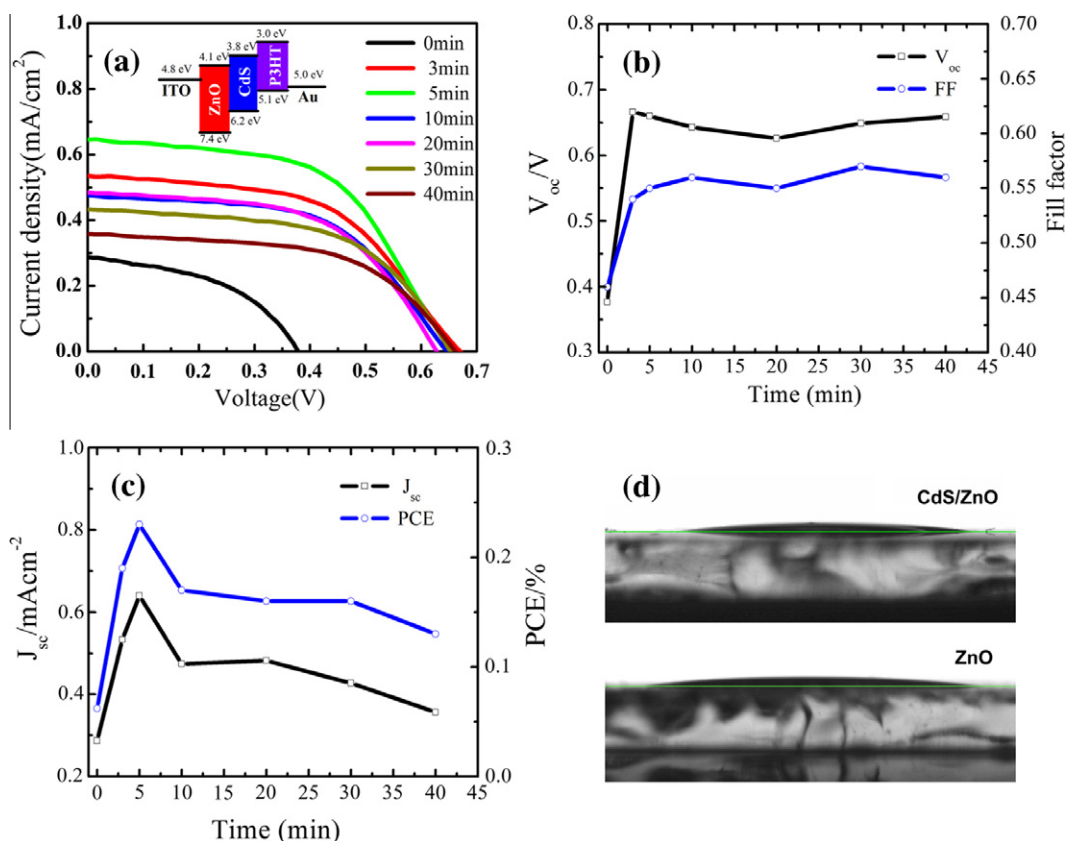
Next, we studied the optimum condition of the CdS modification on ZnO for hybrid solar cells. To simplify the experiments, we have studied the P3HT/CdS/ZnO multilayer photovoltaic devices without nanofibers. Fig. 3(a) shows the current density–voltage ( $J$ - $V$ ) characterizations of the multilayer devices with different CdS growth time. Fig. 3(b) and (c) shows the detailed photovoltaic parameters including short-circuit current density ( $J_{sc}$ ), open circuit voltage ( $V_{oc}$ ), fill factor (FF), and PCE of the devices as functions of CdS growth time. At the beginning, the PCE of a device increases with the increase of CdS growth time. When the growth time is increased to 5 min, the device shows the best performance, yielding a  $J_{sc}$  of 0.64 mA/cm<sup>2</sup>, a  $V_{oc}$  of 660 mV, a FF of 0.55 and a PCE of 0.23%. Then the device performance becomes worse with the increase of growth time when it is over 5 min. Therefore the optimum growth time of CdS layer on ZnO is 5 min, which is the condition for CdS modification in all of our other

experiments, including the SEM and TEM samples shown in Figs. 1 and 2, respectively.

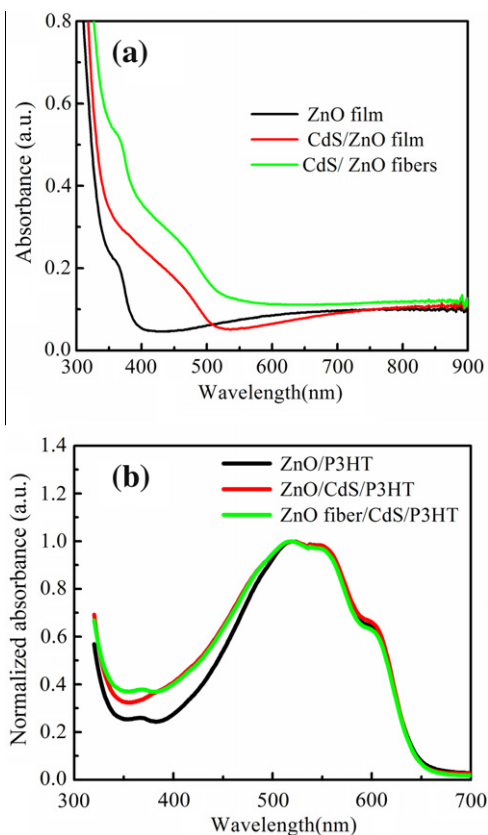
The effect of CdS modification on the performance of the hybrid solar cells can be attributed to the enhanced light absorbance in visible region, the cascaded energy levels and the passivation for traps [9,29]. The band structure of the P3HT/CdS/ZnO heterojunction is shown in Fig. 3(a). The positions of the conduction band and valence band of CdS and the highest occupied molecular orbital (HOMO) and the lowest unoccupied molecular orbital (LUMO) levels of P3HT are favorable for electron injection towards ZnO and hole transport towards P3HT and gold electrode. In addition, the CdS layer also prohibits the recombination of electrons and holes at the interface due to the spatial separation of the two types of carriers, which will be shown in our impedance measurements.

Fig. 4(a) presents the absorption spectra of a ZnO film, a CdS modified ZnO film and CdS modified ZnO nanofibers. Fig. 4(b) shows the normalized absorption spectra of the above three films coated with P3HT layers. The CdS modification obviously increases the light absorption of the composite films in the visible region at the wavelengths less than 500 nm.

Fig. 5(a) shows the  $J$ - $V$  characteristics of the hybrid solar cells based on P3HT and CdS-modified electrospun ZnO nanofibers at various numbers of layers. Fig. 5(b) and (c)



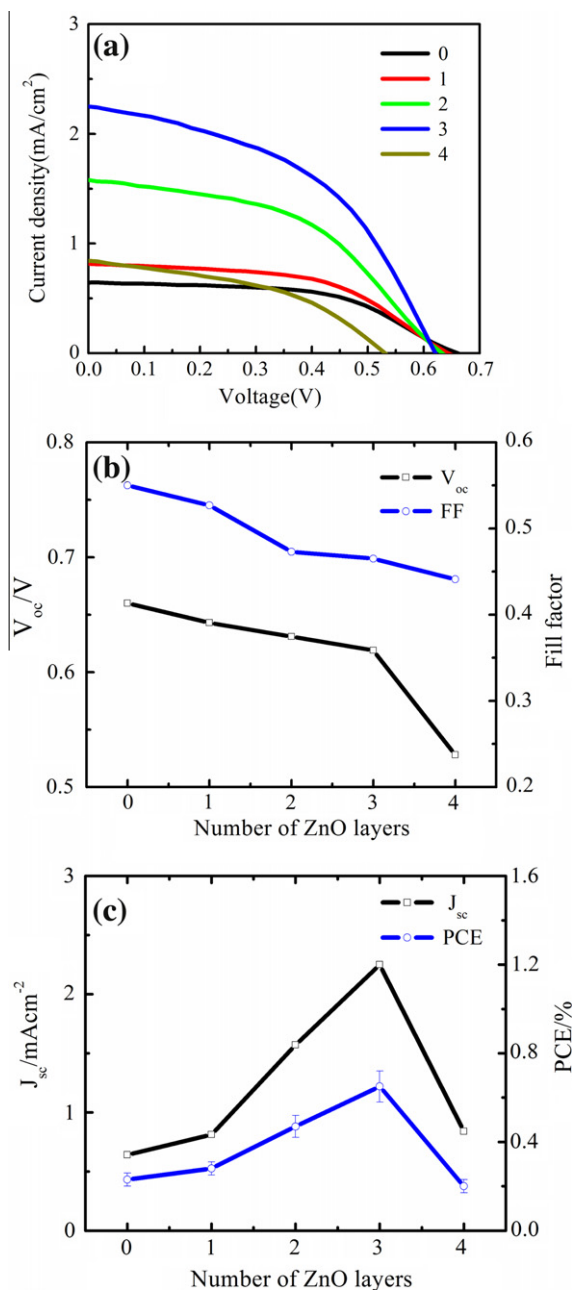
**Fig. 3.** (a) Current–voltage ( $J$ - $V$ ) curves of solar cells based on P3HT and CdS-modified ZnO film (P3HT/CdS/ZnO) with different CdS growth time. Inset: energy band diagram of the hybrid solar cell with the structure of Au/P3HT/CdS/ZnO/ITO. (b) and (c)  $V_{oc}$ , FF,  $J_{sc}$ , and PCE of the P3HT/CdS/ZnO devices as a function of CdS growth time. (d) A drop of toluene on CdS/ZnO (CdS growth time: 5 min) or ZnO film. The contact angles of toluene on both surfaces are  $\sim 10^\circ$ .



**Fig. 4.** Absorbance spectra of ZnO film, CdS modified ZnO film and CdS modified ZnO nanofibrous film before (a) and after (b) the coating of P3HT film. The spectra in (b) were normalized to the P3HT peaks at around 520 nm.

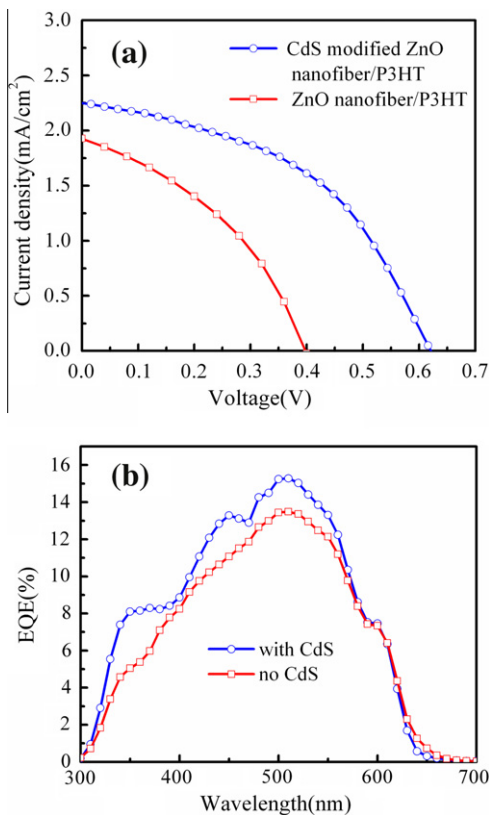
show the detailed photovoltaic parameters including  $J_{sc}$ ,  $V_{oc}$ , FF, and PCE of the devices as functions of the number of layers. We can find that three layers of CdS/ZnO nanofibers can result in the average PCE of  $0.64 \pm 0.07\%$ . The increase of PCE with the increase of the number of cross-aligned layers when it is less than three can be attributed to the increase of P3HT/CdS/ZnO interfacial area and light absorption. However, for the device with four layers of ZnO nanofibers, the thickness of the active layer is too big for such organic solar cells, which normally leads to a low short-circuit current density, a big serial resistance and a low PCE of the device [8,22].

Fig. 6(a) shows the  $J$ - $V$  characteristics of the hybrid solar cells based on P3HT and three layers of ZnO nanofibers with and without CdS modification. The device without CdS modification gives a  $V_{oc}$  of 396 mV, a  $J_{sc}$  of 1.91 mA/cm<sup>2</sup>, a FF of 0.394 and a PCE of 0.3%. The four parameters ( $V_{oc}$ ,  $J_{sc}$ , FF, and PCE) are increased to 619 mV, 2.25 mA/cm<sup>2</sup>, 0.465 and 0.65%, respectively, in the device with CdS modification. It is notable that the improvement of PCE is more than 100%. Fig. 6(b) shows the EQEs of the two devices. It is notable that EQE is improved by CdS modification at both short wavelength (<500 nm) and long wavelength (>500 nm) region. The increase in long wavelength region cannot be attributed to the enhancement of



**Fig. 5.** (a) Current-voltage ( $J$ - $V$ ) curves and (b, c) photovoltaic characteristics of CdS-modified ZnO nanofiber/P3HT hybrid solar cells with different number of cross-aligned ZnO nanofibrous layers.

light absorption induced by CdS layer. Therefore we speculate that the increase of EQE in long wavelength region can be attributed to the effect of CdS layer that prohibits the recombination of electrons and holes at the interface due to the spatial separation of the two types of carriers, which was confirmed by the impedance measurements described in the following part. So the increase of EQE at short wavelength region can be attributed to both the enhanced light absorption shown in Fig. 4(b) and the effect of CdS layer to prohibit carrier recombination.



**Fig. 6.** (a) Current–voltage characteristics and (b) external quantum efficiency (EQE) of hybrid photovoltaic devices with three layers of cross-aligned ZnO nanofibers with or without CdS modification.

It is noteworthy that the improvement of the device performance after the CdS modification may be due to the optimized microstructure of the hybrid films [9,34]. We find that toluene has very little contact angles ( $\sim 10^\circ$ ) on both ZnO and CdS/ZnO films as shown in Fig. 3(d). Therefore, P3HT toluene solution can be infiltrated into both the ZnO and the CdS/ZnO nanofibrous films very well. On other hand, we found that the absorption peaks of P3HT films ( $\sim 520$  nm) on ZnO or CdS/ZnO surface have the same peak positions as shown in Fig. 4(b), indicating that the crystallinity of the P3HT films are very similar on both surfaces [34]. Therefore we consider that the influence of CdS on the morphology (e.g. crystallinity) of P3HT in the hybrid films is negligible.

To better understand the effect of CdS modification on ZnO nanofibers, the impedances of the hybrid solar cells have been characterized at different bias voltages in the dark [8,9,12]. Fig. 7(a) shows the Nyquist plots of the devices with three layers of cross-aligned ZnO nanofibers with and without CdS modification measured at the bias voltage of 0.5 V. It can be found that each curve is composed of two semicircles. As analyzed in the previous paper [8], the left arc can be attributed to the impedance of P3HT/CdS/ZnO or P3HT/ZnO composite film. The right arc corresponds to the charge transfer process at the P3HT/CdS/ZnO or P3HT/ZnO interface. The lifetime of carriers at the interface can be calculated according to the diffusion-recombination

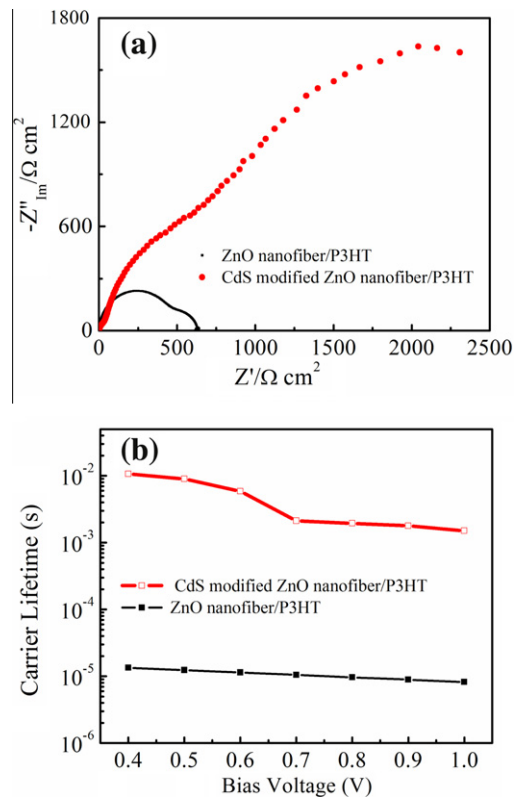


**Fig. 7.** (a) Nyquist plots of the impedance of hybrid solar cells containing three layers of ZnO nanofibers with or without CdS modification measured at the bias voltage of 0.5 V (close to  $V_{oc}$ ). (b) The lifetimes of carriers in the devices with or without CdS modification characterized at different bias voltages in the dark.

model [35,36]. Fig. 7(b) shows the calculated carrier lifetimes of the devices with and without CdS modification under various bias voltages. It is interesting to find that the carrier lifetime is dramatically increased after the CdS modification.

The enhanced carrier lifetime can be attributed to the retarded recombination kinetics due to the surface modification on ZnO nanofibers [8,9,12]. The CdS modifier can not only reduce the recombination centers on the surface but also block the back electron transfer from ZnO to P3HT, resulting in longer carrier lifetime. It is notable that  $V_{oc}$  is strongly influenced by the recombination rate at the heterojunction of a solar cell [9,37]. Lower recombination rate of carriers will lead to a higher open circuit voltage. Therefore, the significant improvements of the  $V_{oc}$  and the PCE of the hybrid solar cells after CdS modification can be understood, which is similar to the effect of surface modification observed in the oxide/P3HT hybrid solar cells reported before [9,12].

#### 4. Conclusions

Hybrid solar cells based on P3HT and electrospun ZnO nanofibers have been fabricated. ZnO nanofibers were modified with CdS to form core-shell CdS/ZnO nanofibers

by solution process. The performance of the hybrid solar cell was dependent on the CdS growth time and the thickness of ZnO nanofibrous layer. The PCEs of the devices were improved from 0.3% to 0.65% after the CdS modification at the optimized fabrication condition, which is attributed to the cascaded band structure of the heterojunction that can facilitate charge transfer at the interface and induce higher light absorption in visible region. The impedance measurements demonstrated that the carrier lifetime at the organic/inorganic heterojunction was prolonged substantially after the surface modification of CdS. Longer lifetime of carriers at the heterojunction can lead to a higher open circuit voltage of the device.

## Acknowledgements

This work is financially supported by the Research Grants Council (RGC) of Hong Kong, China (project number: PolyU5330/08E), the Hong Kong Polytechnic University (project number: J-BB9S and A-PB0M) and the National Natural Science Foundation of China (Grant No. 51003035).

## References

- [1] M.T. Lloyd, Y.J. Lee, R.J. Davis, E. Fang, R.M. Fleming, J.W.P. Hsu, *J. Phys. Chem. C* 113 (2009) 17608.
- [2] Y.Y. Lin, Y.Y. Lee, L. Chang, J.J. Wu, C.W. Chen, *Appl. Phys. Lett.* 94 (2009) 063308.
- [3] W.J.E. Beek, M.M. Wienk, R.A.J. Janssen, *Adv. Funct. Mater.* 16 (2006) 1112.
- [4] Y.Y. Lin, T.H. Chu, S.S. Li, C.H. Chuang, C.H. Chang, W.F. Su, C.P. Chang, M.W. Chu, C.W. Chen, *J. Am. Chem. Soc.* 131 (2009) 3644.
- [5] S.S. Li, Y.Y. Lin, W.F. Su, C.W. Chen, *J. Sel. Top. Quantum Electron.* 16 (2010) 1635.
- [6] S.D. Oosterhout, M.M. Wienk, S.S.V. Bavel, R. Thiedmann, L.J.A. Koster, J. Gilot, J. Loo, V. Schmidt, R.A.J. Janssen, *Nat. Mater.* 8 (2009) 818.
- [7] J. Weickert, R.B. Dunbar, H.C. Hesse, W. Wiedemann, L.S. Mende, *Adv. Mater.* 23 (2011) 1810.
- [8] S. Wu, Q. Tai, F. Yan, *J. Phys. Chem. C* 114 (2010) 6197.
- [9] Q.D. Tai, F. Yan, X.Z. Zhao, *J. Mater. Chem.* 20 (2010) 7366.
- [10] S.M. Mok, F. Yan, H.L.W. Chan, *Appl. Phys. Lett.* 93 (2008) 023310.
- [11] Z.K. Liu, J.H. Li, Z.H. Sun, G.A. Tai, S.P. Lau, F. Yan, *ACS Nano* 6 (2012) 810.
- [12] T.W. Zeng, I.S. Liu, F.C. Hsu, K.T. Huang, H.C. Liao, W.F. Su, *Opt. Express* 18 (2010) A357.
- [13] G.K. Mor, S. Kim, M. Paulose, O.K. Varghese, K. Shankar, J. Basham, C.A. Grimes, *Nano Lett.* 9 (2009) 4250.
- [14] K.M. Coakley, M.D. McGehee, *Appl. Phys. Lett.* 83 (2003) 3380.
- [15] B. Sun, E. Marx, N.C. Greenham, *Nano Lett.* 3 (2003) 961.
- [16] J. Boucle, H.J. Snaith, N.C. Greenham, *J. Phys. Chem. C* 114 (2010) 3664.
- [17] K. Takanezawa, K. Hirota, Q.S. Wei, K. Tajima, K. Hashimoto, *J. Phys. Chem. C* 111 (2007) 7218.
- [18] L.E. Green, M. Law, B.D. Yuhas, P.D. Yang, *J. Phys. Chem. C* 111 (2007) 18451.
- [19] D.C. Olson, S.E. Shaheen, R.T. Collins, D.S. Ginley, *J. Phys. Chem. C* 111 (2007) 16670.
- [20] Y.J. Lee, M.T. Lloyd, D.C. Olson, R.K. Grubbs, P. Lu, R.J. Davis, J.A. Voigt, J.W.P. Hsu, *J. Phys. Chem. C* 113 (2009) 15778.
- [21] D.C. Olsen, Y.J. Lee, M.S. White, N. Kopidakis, S.E. Shaheen, D.S. Ginley, J.A. Voigt, J.W.P. Hsu, *J. Phys. Chem. C* 112 (2008) 9544.
- [22] S.J. Wu, J.H. Li, Q.D. Tai, F. Yan, *J. Phys. Chem. C* 114 (2010) 21873.
- [23] Z.K. Liu, F. Yan, *Phys. Status Solidi RRL* 5 (2011) 367.
- [24] Q.D. Tai, J.H. Li, Z.K. Liu, Z.H. Sun, X.Z. Zhao, F. Yan, *J. Mater. Chem.* 21 (2011) 6848.
- [25] B.R. Lee, H. Choi, J.S. Park, H.J. Lee, S.O. Kim, J.Y. Kim, M.H. Song, *J. Mater. Chem.* 21 (2011) 2051.
- [26] J.A. Chang, J.H. Rhee, S.H. Im, Y.H. Lee, H.J. Kim, S. Seok, M.K. Nazeeruddin, M. Gratzel, *Nano Lett.* 10 (2010) 2609.
- [27] M. Seol, H. Kim, Y. Tak, K. Yong, *Chem. Commun.* 46 (2010) 5521.
- [28] Z. Yang, C.Y. Chen, C.W. Liu, H.T. Chang, *Chem. Commun.* 46 (2010) 5485.
- [29] E.D. Spoeerke, M.T. Lloyd, E.M. Mccready, D.C. Olson, Y.J. Lee, J.W.P. Hsu, *Appl. Phys. Lett.* 95 (2009) 213506.
- [30] Y. Itzhaik, O. Niitsoo, M. Page, G. Hodes, *J. Phys. Chem. C* 113 (2009) 4254.
- [31] E.D. Spoeerke, M.T. Lloyd, Y.J. Lee, T.N. Lambert, B.B. Mckenzie, Y.B. Jiang, D.C. Olson, T.L. Sounart, J.W.P. Hsu, J.A. Voigt, *J. Phys. Chem. C* 113 (2009) 16329.
- [32] H. Tang, F. Yan, Q.D. Tai, H.L.W. Chan, *Biosens. Bioelectron.* 25 (2010) 1646.
- [33] P. Lin, F. Yan, H.L.W. Chan, *Langmuir* 25 (2009) 7465.
- [34] Z.H. Sun, J.H. Li, C.M. Liu, S.H. Yang, F. Yan, *Adv. Mater.* 23 (2011) 3648.
- [35] J. Bisquert, *J. Phys. Chem. B* 106 (2002) 325.
- [36] M. Adachi, M. Sakamoto, J.T. Jiu, Y. Ogata, S. Isoda, *J. Phys. Chem. B* 110 (2006) 13872.
- [37] U. Rau, *Phys. Rev. B* 76 (2007) 085303.